Quantum dynamics of the parametric oscillator

P. Kinsler and P. D. Drummond
Department of Physics, University of Queensland, Queensland 4072, Australia
(Received 5 November 1990)

We present dynamical calculations for the quantum parametric oscillator using both number-state and coherent-state bases. The coherent-state methods use the positive-P representation, which has a nonclassical phase space—an essential requirement in obtaining an exact stochastic representation of this nonlinear problem. This also provides a way to directly simulate quantum tunneling between the two above-threshold stable states of the oscillator. The coherent-state methods provide both analytic results at large photon numbers, and numerical results for any photon number, while our number-state calculations are restricted to numerical results in the low-photon-number regime. The number-state and coherent-state methods give precise agreement within the accuracy of the numerical calculations. We also compare our results with methods based on a truncated Wigner representation equivalent to stochastic electrodynamics, and find that these are unable to correctly predict the tunneling rate given by the other methods. An interesting feature of the results is the much faster tunneling predicted by the exact quantum-theory methods compared with earlier semiclassical calculations using an approximate potential barrier. This is similar to the faster tunneling found when comparing quantum penetration of a barrier to classical thermal activation. The quantum parametric oscillator, which has an exact steady-state solution, therefore provides a useful and accessible system in which nonlinear quantum effects can be studied far from thermal equilibrium.

I. INTRODUCTION

The steady-state behavior of the parametric oscillator has been extensively studied. For the *degenerate* parametric oscillator (DPO), spontaneous switching between the two above-threshold steady states due to thermal noise[1] and tunneling due to quantum noise[2] have been considered. In this paper we present calculations of the mean time taken to tunnel between the states due to quantum noise effects. These results are interesting for several reasons. Quantum systems driven to a steady state far from thermal equilibrium are a subject of much current research. As well as given predictions for tunneling behavior in this environment, our results show that good agreement is obtained between methods using a number-state basis and those using coherent states.

The degenerate parametric oscillator has two regions of operation. When the input laser field (pump) of the fundamental mode is weak, the subharmonic (signal) mode has a zero average amplitude. This is called the *below-threshold* regime. If the pump is sufficiently strong, there are two possible states of the subharmonic field. These have equal intensities but opposite phases. This is the *above-threshold* regime. It is the tunneling between these above-threshold phase states that we consider in this paper. It is important to note that the tunneling considered here is not *coherent* tunneling, often called quantum coherence.[3] The quantum tunneling considered here is similar to that in quantum jump experiments,[4] and is due to quantum effects in a nonequilibrium system. Any coherent tunneling effects in the system we consider will be strongly suppressed by the cavity losses.

The earliest calculation of phase switching in the degenerate parametric oscillator was that of Woo and Landauer.[1] This classical analysis only considered thermal noise sources. The calculation was based on an electrical circuit model, but it is directly analogous to the optical case. Next, Graham's pioneering study[2] of quantum noise analyzed the system using the Wigner representation.[5] This representation uses symmetrically ordered operators, and gives equations that are more "classical" in appearance than the coherent-state representations that we use. After introducing approximations which effectively truncate the exact quantum-mechanical Wigner equation into a semiclassical form, a mean tunneling time result was obtained that was similar in form to the classical result. The only difference was that the noise coefficient included symmetrically ordered vacuum fluctuation terms in the subharmonic mode reservoirs, while neglecting fundamental mode vacuum fluctuations.

Recently, we have obtained analytic results for the mean quantum tunneling time that are significantly different[6,7] from the previous calculations. We use a coherent-state basis for the density operator, which leads to an exact Fokker-Planck equation on a nonclassical phase space,[8] whose tunneling eigenvalue is then obtained asymptotically. In this paper we expand our earlier work and include new calculations using a number-state basis. The number-state calculation gives results that agree with the coherent-state (positive-P representation) analytic theory. However, the number-state calculation does require substantial computational effort to obtain results with even a small photon number.

In addition we have performed a series of numerical simulations using stochastic equations equivalent to the exact positive-P Fokker-Planck equation. As expected, we find that these simulations are in good agreement with the number-state calculations. We have also carried out

numerical simulations using the truncated Wigner Fokker-Planck equations. This was done both for equations that neglect noise in the fundamental mode, and also for a more complete set of equations that included the fundamental mode noise. Neither of the truncated Wigner theories agrees with the exact quantum-mechanical results, except near threshold. Thus the truncated Wigner technique, which is equivalent to stochastic electrodynamics,[9] cannot describe true nonlinear quantum processes. Of most interest is the agreement among all the exact quantum-mechanical equations, which predict much shorter tunneling times well above threshold than given by the earlier semiclassical theories.

II. PHYSICAL MODEL

The behavior of the degenerate parametric oscillator may be formulated in terms of a simple model consisting of an optical cavity and two quantized field modes, one at frequency ω and one at frequency 2ω, which interact via a second-order nonlinearlity. These modes are called the *subharmonic* and *fundamental* modes. Both modes are taken to be resonant with the cavity. Losses at the cavity mirrors for both modes are included, the damping being modeled by using reservoir modes with operators $\hat{\Gamma}_i$ and $\hat{\Gamma}_i^\dagger$. The input pump field has frequency 2ω and is treated classically. The interaction Hamiltonian for this two-mode system is

$$\hat{H}=\tfrac{1}{2}i\hbar[\kappa^*\hat{a}_1^{\,2}\hat{a}_2^{\,\dagger}-\kappa(\hat{a}_1^{\,\dagger})^2\hat{a}_2]+i\hbar(\epsilon\hat{a}_2^{\,\dagger}-\epsilon^*\hat{a}_2)$$
$$+\hat{a}_1\hat{\Gamma}_1^{\,\dagger}+\hat{a}_1^{\,\dagger}\hat{\Gamma}_1+\hat{a}_2\hat{\Gamma}_2^{\,\dagger}+\hat{a}_2^{\,\dagger}\hat{\Gamma}_2\,. \tag{2.1}$$

Here $\hat{a}_1,\hat{a}_1^{\,\dagger}$ and $\hat{a}_2,\hat{a}_2^{\,\dagger}$ are the annihilation and creation operators for the two modes with frequencies ω and 2ω, respectively, and κ is the intermode coupling constant. The first term in the Hamiltonian describes the interaction between the two modes. The classical pump amplitude injected into the fundamental mode at frequency 2ω is ϵ, while the remaining terms describe the losses for the two modes at the cavity mirrors, with decay rates γ_1 and γ_2 for the subharmonic and fundamental modes. The processes described by this Hamiltonian are diagrammatically represented in Fig. 1(a).

When the fundamental mode decays rapidly compared with the subharmonic mode, an alternative and simpler model Hamiltonian can be used. This contains just one quantized electromagnetic field mode at frequency ω, with the annihilation and creation operators $\hat{a}_1$ and $\hat{a}_1^{\,\dagger}$. The Hamiltonian includes both a two-photon coherent pump and a two-photon decay process for the subharmonic mode, in addition to the usual one-photon damping process with a damping rate of γ_1. The coefficients employed are specified by the criterion that the correct classical results must be regained in the classical limit of large numbers of photons and also by comparison with the two-mode model given above. The Hamiltonian for this simple model is then

$$\hat{H}=i\hbar\left[\left[\frac{\kappa\epsilon}{2\gamma_2}\right](\hat{a}_1^{\,\dagger})^2-\left[\frac{\kappa^*\epsilon^*}{2\gamma_2}\right]\hat{a}_1^{\,2}\right]+\hat{a}_1\hat{\Gamma}_1^{\,\dagger}$$
$$+\hat{a}_1^{\,\dagger}\hat{\Gamma}_1+\left[\frac{\kappa\kappa^*}{4\gamma_2^2}\right]\hat{a}_1^{\,2}\hat{\Gamma}_2^{\,\dagger}+\left[\frac{\kappa^*\kappa}{4\gamma_2^2}\right](\hat{a}_1^{\,\dagger})^2\hat{\Gamma}_2\,. \tag{2.2}$$

The two-photon pump strength is $\kappa\epsilon/2\gamma_2$ and the two-photon damping rate is $\kappa^*\kappa/4\gamma_2$. This Hamiltonian can be represented as in Fig. 1(b). The equivalence of this Hamiltonian to the full Hamiltonian in the adiabatic limit will be shown in Sec. IV. We therefore call the Hamiltonian for this system the "adiabatically equivalent Hamiltonian."

Either model described above can be used to obtain a

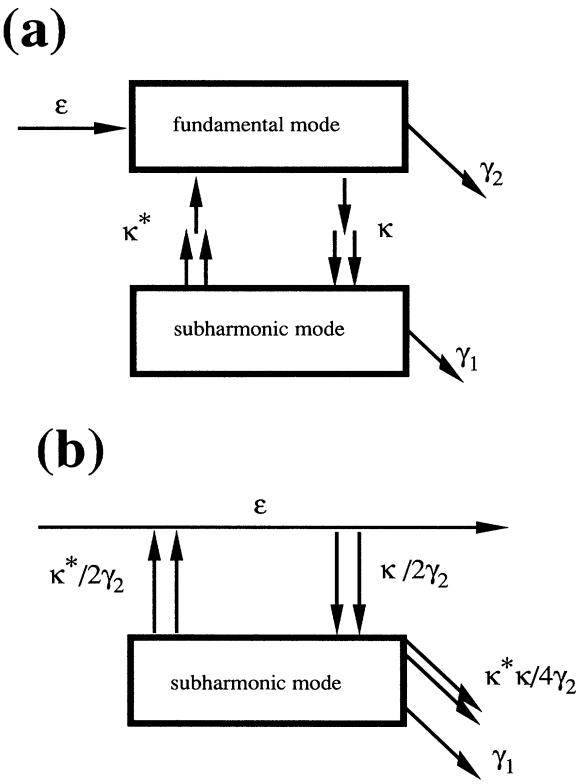

FIG. 1. (a) A diagram representing the two-mode DPO Hamiltonian (2.1). The boxes correspond to the cavity modes. Each arrow represents whether photons are being put into or taken out of the modes, with pairs of arrows denoting pairs of photons. The classical pump puts photons into the fundamental mode at a rate ε. The decay processes remove single photons at rates γ_1 and γ_2 for the subharmonic and fundamental modes, respectively. The nonlinear interaction simultaneously takes single photons out of the fundamental and puts two photons into the subharmonic at a rate κ. This process also occurs in reverse, where two photons are taken out of the subharmonic and one is put into the fundamental. (b) A diagram representing the adiabatically equivalent DPO Hamiltonian (2.2). The same conventions as for (a) are used. Here pairs of photons are put into the subharmonic at a rate $\epsilon\kappa/2\gamma_2$, and removed at a rate $\epsilon^*\kappa^*/2\gamma_2$. There are two decay processes, of both single and pairs of photons, at rates γ_1 and $\kappa^*\kappa/4\gamma_2$.

master equation for the time evolution of the density matrix. From that master equation, a Fokker-Planck equation can be generated that describes the system in terms of the coherent-state basis positive-P representation,[10] which will be treated later, in Sec. IV. In this paper we mostly consider the simpler system that corresponds to the Hamiltonian (2.2). Using standard methods[11] this gives a zero temperature master equation of

$$\frac{d}{dt}\hat{\rho}=L\rho=\left[\left[\frac{\kappa\epsilon}{2\gamma_2}\right](\hat{a}_1^{\dagger})^2-\left[\frac{\kappa^*\epsilon^*}{2\gamma_2}\right]\hat{a}_1^2,\hat{\rho}\right]+\gamma_1(2\hat{a}_1\hat{\rho}\hat{a}_1^{\dagger}-\hat{a}_1^{\dagger}\hat{a}_1\hat{\rho}-\hat{\rho}\hat{a}_1^{\dagger}\hat{a}_1)$$
$$+\left[\frac{\kappa^*\kappa}{4\gamma_2}\right][2\hat{a}_1^2\hat{\rho}(\hat{a}_1^{\dagger})^2-(\hat{a}_1^{\dagger})^2\hat{a}_1^2\hat{\rho}-\hat{\rho}(\hat{a}_1^{\dagger})^2\hat{a}_1^2], \tag{2.3}$$

where L is the superoperator describing the time evolution of the density matrix. By selecting the relative phases of the quantum states, and hence the phase of κ, we can ensure that $\kappa\epsilon=\kappa^*\epsilon^*$ with no loss of generality.[12] We also introduce the scaled variables

$$g^2=\frac{\kappa^*\kappa}{2\gamma_1\gamma_2},\quad \mu=\frac{|\kappa\epsilon|}{\gamma_1\gamma_2},\quad \tau=\gamma_1 t\ . \tag{2.4}$$

Here, g is the coupling constant scaled by the geometric mean of the mode decay rates. The limit $g^2\ll 1$ corresponds to the current experimental limits of large threshold photon numbers. The time τ is measured in cavity lifetimes. Also, μ is the pump amplitude scaled so that the threshold condition of parametric oscillation is at $\mu=1$. Using these, the master equation reduces to

$$\frac{d}{d\tau}\hat{\rho}=\tfrac{1}{2}\mu[(\hat{a}_1^{\dagger})^2-\hat{a}_1^2,\hat{\rho}]+(2\hat{a}_1\hat{\rho}\hat{a}_1^{\dagger}-\hat{a}_1^{\dagger}\hat{a}_1\hat{\rho}-\hat{\rho}\hat{a}_1^{\dagger}\hat{a}_1)$$
$$+\tfrac{1}{2}g^2[2\hat{a}_1^2\hat{\rho}(\hat{a}_1^{\dagger})^2-(\hat{a}_1^{\dagger})^2\hat{a}_1^2\hat{\rho}-\hat{\rho}(\hat{a}_1^{\dagger})^2\hat{a}_1^2]\ . \tag{2.5}$$

This master equation can be treated by expanding in a suitable basis, using number-state or coherent-state methods. These are dealt with in Secs. III and IV, respectively. Alternative techniques, using the Wigner distribution, are treated in Sec. V.

We note here that Eq. (2.5) describes the evolution of a Hilbert-space operator on a phase space of infinite dimension. The nonlinear terms mean that Heisenberg equation methods would result in equations with noncommuting operator products. Perturbation-theory techniques are also difficult to utilize, as all the coefficients can be comparable in size. Thus these relatively standard techniques are not useful in this problem.

III. NUMBER-STATE EXPANSION

An obvious method for solving the master equation is to simply expand Eq. (2.5) over a number-state basis. The number states are an orthogonal, complete basis for the harmonic-oscillator Hilbert space. In this basis the master equation reduces to an infinite matrix equation. However, as any physical system must have a finite energy, a suitable energy cutoff will reduce the system to a finite number of elements. The system can then be treated numerically.

We first expand $\hat{\rho}$ in terms of its number-state matrix elements $\rho(n,m)$. These are defined by

$$\rho(n,m)=\langle n|\hat{\rho}|m\rangle\ . \tag{3.1}$$

Thus, in the number-state basis, the time evolution is given by

$$\frac{d}{dt}\rho(n,m)=\left\langle n\left|\frac{d}{dt}\hat{\rho}\right|m\right\rangle\ . \tag{3.2}$$

The equation for $d\rho(n,m)/dt$ can be written in matrix form using the Einstein summation convention on identical indices. We write $\rho(i,j)$ as ρ_{ij} and introduce the four-dimensional transition matrix T_{ij}^{nm} to describe the time evolution of ρ_{ij}. Each element of this supermatrix T_{ij}^{nm} is the rate of transition from the state ρ_{nm} to the state ρ_{ij}. A positive rate implies that there is a flow of probability into the state, and a negative rate means a flow out of the state. The indices $(ijnm)$ span the range of possible photon numbers, zero to infinity. Using this notation, Eq. (2.5) becomes

$$\frac{d}{d\tau}\rho_{ij}=T_{ij}^{nm}\rho_{nm}\ . \tag{3.3}$$

The supermatrix T_{ij}^{nm} is defined by

$$T_{ij}^{nm}=\tfrac{1}{2}\mu\sqrt{i(i-1)}\delta_{i;j}^{n+2;m}+\tfrac{1}{2}\mu\sqrt{j(j-1)}\delta_{i;j}^{n;m+2}-\tfrac{1}{2}\mu\sqrt{(i+1)(i+2)}\delta_{i;j}^{n-2;m}-\tfrac{1}{2}\mu\sqrt{(j+1)(j+2)}\delta_{i;j}^{n;m-2}$$
$$-\{(i+j)+g^2[i(i-1)+j(j-1)]\}\delta_{i;j}^{n;m}+2\sqrt{(i+1)(j+1)}\delta_{i;j}^{n-1;m-1}$$
$$+g^2\sqrt{(i+1)(i+2)(j+1)(j+2)}\delta_{i;j}^{n-2;m-2} \tag{3.4}$$

where

$$\delta_{i;j}^{n;m}=\begin{cases}1 & \text{if } i=n \text{ and } j=m\\ 0 & \text{otherwise}\ .\end{cases}$$

The behavior of the system can be characterized in terms of the eigenvalues and eigenvectors of the transition matrix $\underline{T}$. The eigenvector corresponding to the zero eigenvalue is the steady state of the system. The tunnel-

ing eigenvalue is the smallest negative nonzero eigenvalue. However, before the eigenvalues and eigenvectors can be calculated numerically, the problem must be made finite. That is, we must place some limit on the maximum photon number allowed. This type of approximation will be valid if the high-proton-number states that are ignored play no significant role in determining the evolution of the system. Thus, by choosing the parameters and a photon number cutoff N to suit these requirements, accurate calculations can be performed.

In addition to this truncation, we must reduce the four-dimensional matrix $\underline{T}$ to two dimensions so that standard eigenvalue and eigenvector software routines can be used. As a consequence the two-dimensional density matrix ρ is also reduced to one dimension. The reduction in dimensions is achieved by stacking the columns of ρ on top of one another, thus converting it into a column vector. A similar process transforms the transition matrix $\underline{T}$ into a two-dimensional matrix. Using Greek indices to indicate the change, we can now write (3.3) as

$$\frac{d}{d\tau}\rho_\alpha = T^\beta_\alpha \rho_\beta \ . \tag{3.5}$$

The new transition matrix is given by

$$T^\beta_\alpha = \tfrac{1}{2}\mu\sqrt{i(i-1)}\,\delta^{\alpha+2N+2}_\beta + \tfrac{1}{2}\mu\sqrt{j(j-1)}\,\delta^{\alpha+2}_\beta - \tfrac{1}{2}\mu\sqrt{(i+1)(i+2)}\,\delta^{\alpha-2N-2}_\beta - \tfrac{1}{2}\mu\sqrt{(j+1)(j+2)}\,\delta^{\alpha-2}_\beta$$
$$-\{(i+j)+g^2[i(i-1)+j(j-1)]\}\delta^\alpha_\beta + 2\sqrt{(i+1)(j+1)}\,\delta^{\alpha-N-1}_\beta + g^2\sqrt{(i+1)(i+2)(j+1)(j+2)}\,\delta^{\alpha-2N-4}_\beta \tag{3.6}$$

where

$$\alpha = (N+1)n + m \quad (0 \le n,m \le N) \ ,$$
$$\beta = (N+1)i + j, \quad (0 \le n,m \le N) \ .$$

Here δ^α_β is a Kronecker delta, but care does not have to be taken to ensure that the $(ijnm)$ used to calculate α and β are in the range $0-N$. The nonzero elements of the new two-dimensional transition matrix form seven bands parallel to its diagonal. This new matrix is *not* Hermitian (i.e., not symmetric, since its elements are real) because of the one- and two-photon damping terms. The eigenvectors of nonzero eigenvalues do not on their own correspond to physical states of the system, any physical state being a combination of the ground-state eigenvector with a sum of other eigenvectors. Thus, as time passes, the contribution due to the decaying eigenvectors becomes zero, leaving just the ground-state eigenvector. In addition, not all of the numerically calculated orthogonal eigenvectors are symmetric (Hermitian) in the (nm) basis. However, these occur in transpose pairs with equal eigenvalues, so that Hermitian eigenvectors can be constructed.

We label the kth eigenvalue by λ_k and its corresponding eigenvector by $\rho^{(k)}_\alpha$ so that

$$\rho_\alpha(\tau) = \sum_{k \ge 0} A_k \exp(\lambda_k \tau)\rho^{(k)}_\alpha \ . \tag{3.7}$$

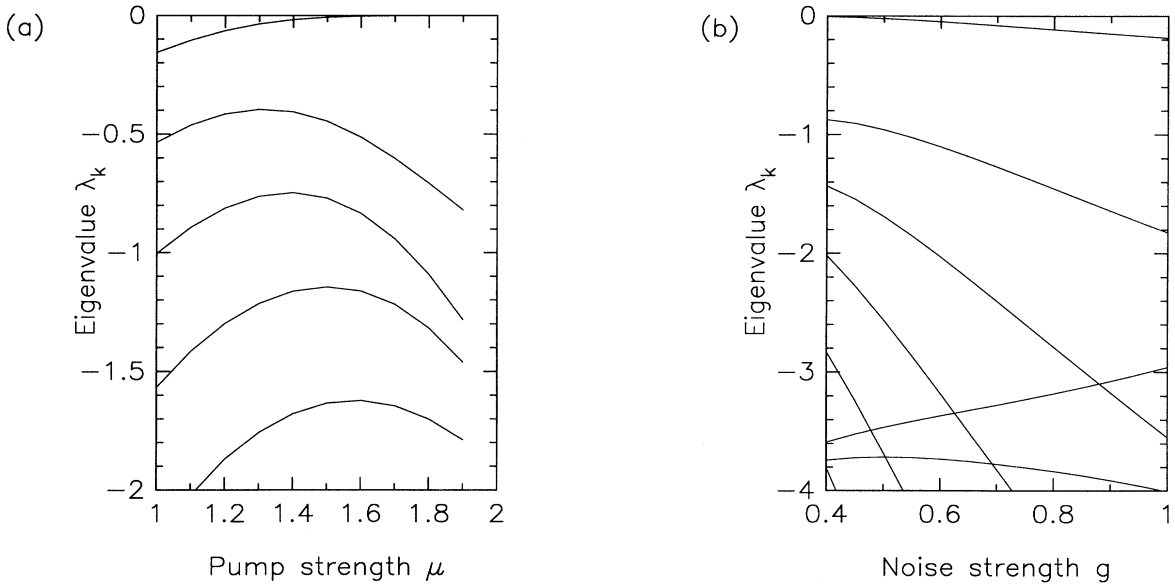

FIG. 2. Graphs of the eigenvalue spectra obtained from the transition matrix $\underline{T}$. In (a), the pump strength μ is varied while the noise strength $g = 0.25$, and in (b) the noise strength g is varied while the pump strength $\mu = 2.00$. Only the smallest few eigenvalues are shown.

Here the coefficients A_k define the initial state. We order the indices k by the size of the real part of the eigenvalue, so that $\mathrm{Re}(\lambda_k) \geq \mathrm{Re}(\lambda_{k+1})$. Thus λ_0 is the stable eigenvalue ($\lambda_0=0$) and $\rho_\alpha^{(0)}$ is the stable state. We call λ_1 the tunneling eigenvalue. Higher indices, $k>1$, represent the other dynamics of the system that characterize fluctuations on shorter time scales.

Specific results from these numerical calculations are compared with results obtained using coherent-state basis methods in Sec. IV. Typical results are presented in Fig. 2, where the smallest few eigenvalues are plotted as both pump strength μ and coupling (noise strength) g vary. They demonstrate the characteristic of quantum tunneling, that there is an isolated eigenvalue near the ground-state eigenvalue, with all other eigenvalues much larger in magnitude. Unlike coherent tunneling, these eigenvalues are real rather than imaginary. This is due to the presence of decay processes modeled by the reservoirs, and reflects the fact that we are treating the dynamics of an open rather than a closed quantum system.

We denote the mean tunneling time obtained from these numerical procedures as T_N. Here T_N is defined as the mean switching time of a two-state random telegraph signal that has the same decay rate of amplitude as the tunneling eigenvector. Thus T_N is related to the dimensionless tunneling eigenvalue λ_1 to

$$\gamma_1 T_N = -\frac{2}{\lambda_1} . \tag{3.8}$$

Details of the numerical procedures used are given in Appendix A. More than one software package was employed to ensure software reliability, and a number of checks on precision and accuracy were used. This method was successful for relatively large coupling g and small pump strength μ, where there are small numbers of photons involved. This allowed truncations with around $N=40$ photon number states, giving transition matrix sizes of 40^4 elements or less. However, the diagonalization method is not useful for the typical photon numbers of $N=10^6$ found in many current experiments. The scaling is even less favorable for multimode situations, where the transition matrix has N^{4m} elements for m modes.

In summary, the number-state expansion method is only useful for treating small numbers of photons, due to the memory limitations of computers—and this is unlikely to improve quickly since the size of the transition matrix grows explosively with increasing maximum photon number.

IV. COHERENT-STATE POSITIVE-P REPRESENTATION

Because the number-state methods are less useful at large photon numbers, it is necessary to use alternative techniques to study the parametric oscillator in this region. An obvious alternative is to use a coherent-state[13] basis. These states are especially of merit in the classical limit of electromagnetic fields, as pointed out by Glauber[14] and by Sudarshan.[15] The fact that operators acting on coherent states have particularly straightforward representations in differential form allows for the resulting equations of motion to be solved even in nonclassical regions. Here, due to nonclassical photon statistics, an off-diagonal expansion of $\hat{\rho}$ in terms of coherent states is used. Generalized P representations are normally ordered representations of this type. They have been widely and successfully used[10,16–19] to predict the quantum behavior of the parametric oscillator, as well as that found in four-wave mixing,[20] where squeezing was first observed.[21]

The positive-P representation is defined by[8]

$$\hat{\rho}=\int\int P(\alpha,\alpha^\dagger)\frac{|\alpha\rangle\langle\alpha^{\dagger *}|}{\langle\alpha^{\dagger *}|\alpha\rangle}d^2\alpha\, d^2\alpha^\dagger . \tag{4.1}$$

From this expansion, the master equation (2.5) can be transformed into an equivalent Fokker-Planck equation for the quasidistribution function $P(\alpha,\alpha^\dagger)$, by using partial integration. We note that the boundary terms are normally assumed to vanish in transforming to the Fokker-Planck equation form. However, Smith and Gardiner[22] have pointed out the existence of anomalous results for the case of large nonlinear damping, in a master equation similar to ours. These involve diverging trajectories that occur for the coupling (noise strength) $g>1$, leading to nonvanishing boundary terms. For these values of g, nonlinear effects dominate even when the mean photon number is less than 1. This requires nonlinearities many orders of magnitude above those currently achievable in experiment. Accordingly, we restrict our results to $g<1$, where trajectories are always stable.

With the assumption of vanishing boundary terms, we obtain

$$\frac{d}{d\tau}P(\alpha,\alpha^\dagger,\tau)=L_P P(\alpha,\alpha^\dagger,\tau)=\left[\frac{\partial}{\partial\alpha}[\alpha-\alpha^\dagger(\mu-g^2\alpha^2)]+\frac{\partial}{\partial\alpha^\dagger}\{\alpha^\dagger-\alpha[\mu-g^2(\alpha^\dagger)^2]\}+\frac{\partial^2}{\partial\alpha^2}(\mu-g^2\alpha^2)\right.$$
$$\left.+\frac{\partial^2}{\partial(\alpha^\dagger)^2}[\mu-g^2(\alpha^\dagger)^2]\right]P(\alpha,\alpha^\dagger,\tau) . \tag{4.2}$$

The complex variables α and $\alpha^\dagger$ are independent as a consequence of the positive-P representation. Since $\hat{\rho}$ is related to P by a time-independent mapping, all the eigenvectors of the Fokker-Planck operator L_P that correspond to nonzero operators must have eigenvalues identical to those of the superoperator L and transition matrix $\underline{T}$.

Equation (4.2) is in turn equivalent to a pair of Ito stochastic differential equations[23] for the α and $\alpha^\dagger$ coordinates,

$$d\alpha=[-\alpha+\alpha^{\dagger}(\mu-g^2\alpha^2)]d\tau+(\mu-g^2\alpha^2)^{1/2}dZ_1 ,$$
$$d\alpha^{\dagger}=\{-\alpha^{\dagger}+\alpha[\mu-g^2(\alpha^{\dagger})^2]\}d\tau+[\mu-g^2(\alpha^{\dagger})^2]^{1/2}dZ_2 , \tag{4.3}$$

where

$$\langle dZ_i(t)dZ_j(t')\rangle=\delta_{ij}\delta(t-t') .$$

The terms dZ_1 and dZ_2 are independent δ-correlated real-noise variables with a Gaussian probability distribution.[23] Equation (4.3) has been obtained earlier using adiabatic elimination techniques[10] starting from the two-mode Hamiltonian (2.1). This demonstrates that our initial Hamiltonian is adiabatically equivalent to the two-mode problem in the limit $\gamma_2 \gg \gamma_1$. An independent proof of this equivalence, using master equation techniques, was recently obtained by Mortimer and Risken.[24]

As shown by Wolinsky and Carmichael,[25] the dynamical evolution of the α and $\alpha^{\dagger}$ variables is simplified by the existence of a bounded subspace of the four-dimensional phase space in which any stochastic trajectory can be trapped. Suppose a trajectory starts within the manifold $\Lambda(\alpha,\alpha^{\dagger})$ defined by

$$\Lambda(\alpha,\alpha^{\dagger})=\{|g\alpha|\le\sqrt{\mu},|g\alpha^{\dagger}|\le\sqrt{\mu}\} . \tag{4.4}$$

Here both α and $\alpha^{\dagger}$ are restricted to *real* values. Inspection of the terms in Eq. (4.3) shows that both the drift and noise terms remain real, so that the trajectory must stay on the real plane. The trajectory is prevented from crossing the boundaries at $|g\alpha|=\sqrt{\mu}$, $|g\alpha^{\dagger}|=\sqrt{\mu}$ because on the boundary the transverse noise component vanishes. Thus the trajectory must follow the deterministic flow inwards, or be driven along the boundary by the parallel noise component. This ensures that the trajectories will be stable, provided their starting position is within the bounded manifold. The initial quantum state is taken to be the vacuum state, which is within this manifold since it is at the origin.

Equation (4.2) has a corresponding potential $V(\alpha,\alpha^{\dagger})$ and a steady-state probability distribution $P_{\rm SS}(\alpha,\alpha^{\dagger})$ given by

$$V(\alpha,\alpha^{\dagger})=-2\alpha\alpha^{\dagger}-\frac{\sigma}{g^2}\{\ln(\mu-g^2\alpha^2)+\ln[\mu-g^2(\alpha^{\dagger})^2]\} ,$$

and

$$P_{\rm SS}(\alpha,\alpha^{\dagger})=N\exp[-V(\alpha,\alpha^{\dagger})]=N\{(\mu-g^2\alpha^2)[\mu-g^2(\alpha^{\dagger})^2]\}^{1/g^2-1}\times\exp(2\alpha\alpha^{\dagger}) , \tag{4.5}$$

where $\sigma=1-g^2$, and N is a normalization constant. We note that in the case where the noise strength (i.e., the coupling) $g<1$, this exact steady-state distribution has vanishing boundary terms, in accordance with our assumption when deriving the Fokker-Planck equation.

The critical points of this potential correspond to its local maxima, minima, and saddle points. The minima are particularly of interest as the system is most likely to be in the region of these points. To find the critical points, the equations

$$\frac{\partial V}{\partial\alpha}=0 , \quad \frac{\partial V}{\partial\alpha^{\dagger}}=0 \tag{4.6}$$

are solved simultaneously for α and $\alpha^{\dagger}$. Then the second derivatives of the potentials are used to determine the character of these critical points. Evaluating the first derivative of the potential gives the critical points as

$$g\alpha_0=\pm\sqrt{\mu-\sigma}, \quad g\alpha_0^{\dagger}=\pm\sqrt{\mu-\sigma}$$

or

$$g\alpha_0=\pm\sqrt{\mu+\sigma}, \quad -g\alpha_0^{\dagger}=\pm\sqrt{\mu+\sigma} . \tag{4.7}$$

In addition, the point $(g\alpha,g\alpha^{\dagger})=(0,0)$ is a critical point. Above threshold, and for $\sigma>0$ (that is, for the noise strength $g<1$), both α_0 and $\alpha_0^{\dagger}$ have the same sign on the manifold $\Lambda(\alpha_0,\alpha_0^{\dagger})$. The critical points on $\Lambda(\alpha,\alpha^{\dagger})$ for small noise above threshold are therefore given by

$$(g\alpha_0,g\alpha_0^{\dagger})=\pm(\sqrt{\mu-\sigma},\sqrt{\mu-\sigma})$$

or

$$(g\alpha_0,g\alpha_0^{\dagger})=(0,0) . \tag{4.8}$$

Evaluation of the second derivatives of $V(x,y)$ shows that for small noise strength g the point (0,0) is a saddle point and that the other two are potential minima. The main point of interest here is that above threshold (that

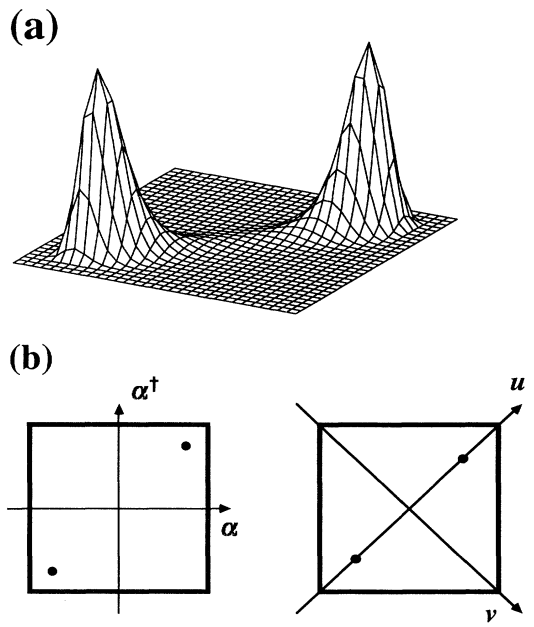

FIG. 3. (a) An example of the above-threshold steady-state probability distribution $P(\alpha,\alpha^{\dagger})$ obtained using the positive-P representation [Eq. (4.5)] on the bounded manifold. The pump strength is $\mu=1.50$ and the noise strength $g=0.25$. (b) The squares denote the edges of the manifolds $\Lambda(\alpha,\alpha^{\dagger})$ and $\Lambda'(u,v)$. The dots indicate the locations of the above-threshold steady states.

is, for pump strength $\mu > 1$) the steady-state probability distribution $P_{SS}(\alpha,\alpha^\dagger)$ has two peaks, corresponding to the two "phase states" the device is most likely to be in. Figure 3(a) shows a typical steady-state probability distribution.

It is useful to transform the equations so that the diffusion or noise terms become constant. Simultaneously with this we rotate the directions of the axes by 45° so that one axis lies along the line between the two steady-state probability distribution peaks. New variables u and v are defined in terms of α and $\alpha^\dagger$ by

$$u=\sin^{-1}\left[\frac{g\alpha}{\sqrt{\mu}}\right]+\sin^{-1}\left[\frac{g\alpha^\dagger}{\sqrt{\mu}}\right],$$
$$v=\sin^{-1}\left[\frac{g\alpha}{\sqrt{\mu}}\right]-\sin^{-1}\left[\frac{g\alpha^\dagger}{\sqrt{\mu}}\right]. \tag{4.9}$$

How these new variables relate to the original variables can be seen in Fig. 3(b). Referring back to the original variables $\alpha,\alpha^\dagger$ it can be seen that in the new variables u and v the line $v=0$ is equivalent to the line $\alpha=\alpha^{\dagger *}$. This line represents the classical subspace of the phase space. Thus the variable v is a nonclassical dimension which allows quantum-mechanical effects to occur.

The bounded manifold $\Lambda(\alpha,\alpha^\dagger)$ has a counterpart in the new variables u and v. It is

$$\Lambda'(u,v)=\{|u|+|v|\leq\pi;\ u,v \text{ real}\} \tag{4.10}$$

This manifold exists for noise strength $g<\sqrt{2}$, the altered noise bound being caused by the change of variables. The Fokker-Planck equation and Ito stochastic differential equations in the variables α and $\alpha^\dagger$ can be transformed into the new variables. The new Fokker-Planck equation is

$$\frac{\partial}{\partial\tau}P'(u,v,\tau)=\left[-\frac{\partial}{\partial u}\left\{\mu\sin(u)-\bar{\sigma}\left[\tan\left[\frac{u+v}{2}\right]+\tan\left[\frac{u-v}{2}\right]\right]\right\}\right.$$
$$\left.-\frac{\partial}{\partial v}\left\{-\mu\sin(v)-\bar{\sigma}\left[\tan\left[\frac{u+v}{2}\right]-\tan\left[\frac{u-v}{2}\right]\right]\right\}+\frac{\partial^2}{\partial u^2}g^2+\frac{\partial^2}{\partial v^2}g^2\right]P'(u,v,\tau), \tag{4.11}$$

where $\bar{\sigma}=1-g^2/2$.

The corresponding Ito stochastic differential equations are

$$du=\left\{\mu\sin(u)-\bar{\sigma}\left[\tan\left[\frac{u+v}{2}\right]+\tan\left[\frac{u-v}{2}\right]\right]\right\}d\tau+\sqrt{2}g\,dZ_u,$$
$$dv=\left\{-\mu\sin(v)-\bar{\sigma}\left[\tan\left[\frac{u+v}{2}\right]-\tan\left[\frac{u-v}{2}\right]\right]\right\}d\tau+\sqrt{2}g\,dZ_v. \tag{4.12}$$

From the Fokker-Planck equation (4.11) an expression for the tunneling time can be developed. Note that, despite appearances, these equations are not periodic in u and v due to the trigonometric functions. Their range is restricted from $-\pi/2$ to $+\pi/2$ by the definitions of u and v in terms of the inverse sine function. The transformed Fokker-Planck equation has the potential solution

$$U(u,v)=-2\bar{\sigma}\ln|\cos(u)+\cos(v)|+\mu\cos(u)-\mu\cos(v), \tag{4.13}$$

and the steady-state probability distribution is given by the equation

$$P'_{SS}(u,v)=N'\exp[-U(u,v)/g^2]. \tag{4.14}$$

The critical points of the potential in the u and v variables are found where the gradient of the potential is zero. In the case where the noise strength g is small, $\bar{\sigma}<1$, and the pump strength is above the threshold level ($\mu>1$), the critical points are found along the line $v=0$. They are located at

$$(u_0,v_0)=(0,0),$$
$$(u_0,v_0)=\left[\pm 2\sin^{-1}\left[\frac{\sqrt{\mu-\bar{\sigma}}}{\sqrt{\mu}}\right],0\right]. \tag{4.15}$$

Here, as for the α and $\alpha^\dagger$ variables the (0,0) critical point is a saddle point and the other two are potential minima. This is shown by calculating the second derivatives of the potential in the variables u and v

$$U_{uu}(u,v)=\frac{\partial^2}{\partial u^2}U(u,v)$$
$$=\tfrac{1}{2}\bar{\sigma}\left[\sec^2\left[\frac{u+v}{2}\right]+\sec^2\left[\frac{u-v}{2}\right]\right]$$
$$-\mu\cos(u),$$
$$U_{vv}(u,v)=\frac{\partial^2}{\partial v^2}U(u,v) \tag{4.16}$$
$$=\tfrac{1}{2}\bar{\sigma}\left[\sec^2\left[\frac{u+v}{2}\right]+\sec^2\left[\frac{u-v}{2}\right]\right]$$
$$+\mu\cos(v).$$

Thus, above threshold, the potential has the form of two wells, each about one of the potential minima. These wells have a "valley" connecting them over the saddle

point. The difference between the value of the potential $U(u,v)$ at the saddle point and the minima is called the potential barrier height. An important feature is that if the noise strength g is not too large and $v=0$, the second derivative in the v direction $U_{vv}(u,0)$ is always positive. Thus the classical subspace is at a minimum of the potential with respect to variations in the nonclassical variable v. This "valley" along the line $v=0$ between the two potential wells is the most likely path for a stochastic trajectory to take when tunneling from one well to the other. The tunneling rate between them will be dominated by the rate due to trajectories traveling along this route, just as it is for the corresponding classical system driven by classical phase space noise sources. However, the actual potential is now substantially different from the classical case.

The stationary-state probability distribution in the new variables u and v now remains zero on the boundary of the manifold for noise strength $g<\sqrt{2}$ rather than just for $g<1$ as in the case of the α and $\alpha^\dagger$ variables. This is a result of the change of variables, as can be seen from the Jacobean of the variable transformation

$$J=\begin{vmatrix} \frac{\partial\alpha}{\partial u} & \frac{\partial\alpha}{\partial v} \\ \frac{\partial\alpha^\dagger}{\partial u} & \frac{\partial\alpha^\dagger}{\partial v} \end{vmatrix} = \tfrac{1}{2}(\mu-g^2\alpha^2)^{1/2}[\mu-g^2(\alpha^\dagger)^2]^{1/2} . \tag{4.17}$$

The two probability distributions are related by

$$P'_{SS}(u,v)=JP_{SS}(\alpha,\alpha^\dagger) = \{(\mu-g^2\alpha^2)[\mu-g^2(\alpha^\dagger)^2]\}^{1/g^2-1/2}\exp(2\alpha\alpha^\dagger) . \tag{4.18}$$

So these new variables u and v not only provide constant diffusion, but also give a finite probability distribution over a larger range of the noise strength g than previously.

The tunneling time for a symmetric bistable potential in two dimensions can be calculated using an extension of the Kramers method developed by Landauer and Swanson.[26] Here we call this method the "potential-barrier approximation." This name arises from the fact that it is valid in the limit where the potential barrier is large. The result for the potential $U(u,v)$ and diffusion g^2 when the saddle point is at (0,0) and the minimum is at (u_0,v_0) is

$$T=2\pi\left[\frac{U_{vv}(0,0)}{U_{vv}(u_0,v_0)U_{uu}(0,0)U_{uu}(u_0,v_0)}\right]^{1/2} \times\exp\left[\frac{U(u_0,v_0)-U(0,0)}{g^2}\right] . \tag{4.19}$$

For the case considered here the potential terms are

$$U(0,0)=-2\bar{\sigma}\ln|2| ,$$
$$U(u_0,v_0)=-2\bar{\sigma}\ln|2|-2\left[\mu-\bar{\sigma}-\bar{\sigma}\ln\left|\frac{\mu}{\bar{\sigma}}\right|\right] . \tag{4.20}$$

The potential curvature terms are

$$U_{uu}(0,0)=-\mu+\bar{\sigma} ,$$
$$U_{vv}(0,0)=\mu+\bar{\sigma} ,$$
$$U_{uu}(u_0,v_0)=2(\mu-\bar{\sigma}) ,$$
$$U_{vv}(u_0,v_0)=2\mu . \tag{4.21}$$

Using the formula (4.19), the tunneling time in the potential-barrier approximation using the positive-P representation is therefore

$$T_p=\frac{\pi}{\gamma_1}\left[\frac{\mu+\bar{\sigma}}{\mu(\mu-\bar{\sigma})^2}\right]^{1/2}\exp\left[\frac{2}{g^2}[\mu-\bar{\sigma}-\bar{\sigma}\ln(\mu/\bar{\sigma})]\right] . \tag{4.22}$$

This is the average time taken for the oscillator to switch from the region of one state (the $u_0>0$ state, for example) to the other due to the influence of quantum noise in the limit of small g. It is inversely proportional to the tunneling eigenvalue λ_1,

$$\gamma_1 T_p=-\frac{2}{\lambda_1} . \tag{4.23}$$

These calculations using the analytic potential-barrier approximation are strictly valid only in the small-g^2 limit. This is the limit of small noise strength and large threshold photon number. Thus these results are valid in the region of most experimental interest. However, it would be useful to have a computational method valid for the whole range of the noise strength $g<1$ rather than only for $g^2\ll 1$. This is provided by the direct simulation of the relevant stochastic equation, i.e., Eqs. (4.12). The eigenvalue is then obtained by fitting an exponential to the decay of the mean amplitude. The size of any possible boundary terms can also be checked during these numerical simulations. Since no trajectories crossed the boundary of the manifold in our simulations, we can say that the boundary terms are zero to within numerical accuracy. Details are given in Appendix B.

Figures 4(a) and 4(b) show an excellent agreement between the number-state calculations, the positive-P stochastic simulations, and the corresponding potential-barrier approximation theory. The simulation results have error bars, which result from the use of a finite sample of trajectories. In the region where the potential-barrier approximation is invalid (small pump strength μ, or large noise g), the predicted tunneling time diverges and no longer agrees with the exact methods. This is due to the reduced size of the potential barrier. The time taken to do either the number-state calculations or the stochastic simulations grows much larger as the mean tunneling time increases. This is because the number-state calculations typically require larger matrices, while the simulations require a much longer run time so that enough of the increasingly rare tunneling events occur to give a good average.

In the experimentally attainable region of relatively large photon numbers, only the coherent-state methods give results—the simulations being more useful in the

critical region in threshold, where the pump strength $\mu \approx 1$, and the analytic theory being applicable for slow tunneling far above threshold, with pump strength $\mu \gg 1$.

V. WIGNER REPRESENTATION

An alternative representation in common use is the symmetrically ordered Wigner representation. Again, all the nontrivial eigenvectors of the superoperator L and the positive-P Fokker-Planck operator L_P should have the same eigenvalues as the spectrum of the Wigner time evolution operator L_W, since the Wigner distribution is obtainable by transforming the P distribution.[27,28] The time evolution equation for the Wigner function is given by Graham.[2] An approximate equation is obtained by first truncating the third-order derivative terms from the coupled-mode equation to get a standard Fokker-Planck equation for the behavior of the fundamental and subharmonic modes:

$$\frac{d}{dt}W_T(\beta_1,\beta_2,t)=\left[\frac{\partial}{\partial\beta_1}(\gamma_1\beta_1-\kappa\beta_1^*\beta_2)+\frac{\partial}{\partial\beta_1^*}(\gamma_1\beta_1^*-\kappa^2\beta_1\beta_2^*)+\frac{\partial}{\partial\beta_2}(\gamma_2\beta_2-\epsilon+\tfrac{1}{2}\kappa^*\beta_1^2)\right.$$
$$\left.+\frac{\partial}{\partial\beta_2^*}[\gamma_2\beta_2^*-\epsilon^*+\tfrac{1}{2}\kappa(\beta_1^*)^2]+\frac{\partial^2}{\partial\beta_1\partial\beta_1^*}(\gamma_1)+\frac{\partial^2}{\partial\beta_2\partial\beta_2^*}(\gamma_2)\right]W_T(\beta_1,\beta_2,t)\ . \tag{5.1}$$

This Fokker-Planck equation is equivalent to a stochastic process and can be written in terms of stochastic differential equations. These equations have a simple physical interpretation in terms of classical phase-space behavior. They are exactly equivalent to a classical degenerate parametric amplifier that is being driven by a coherent pump field and vacuum noise corresponding to half a thermal photon in each external reservoir. This can be considered equivalent to a stochastic electrodynamics-type calculation,[9] which uses this assumption to simulate vacuum fluctuations. Despite the approximations, these equations have the useful feature that they can be readily simulated, and have behavior very similar to the classical parametric oscillator in the presence of finite temperature reservoirs. They also give correct results for small linear fluctuations, when they are compared to previous predictions.[10,29,30]

It has been noted by one of us[31] that the effect of dropping of higher-order derivative terms in Fokker-Planck equations is highly dependent on the choice of representation. Although it is often a good approximation for linear fluctuations, it can change switching times by many orders of magnitude, so this approximation is inherently problematic. However, it is necessary for the Wigner case if standard Fokker-Planck or stochastic methods are to be used. This is because the Wigner time evolution equation, with its third-order derivatives, has the possibility of acquiring negative values. By compar-

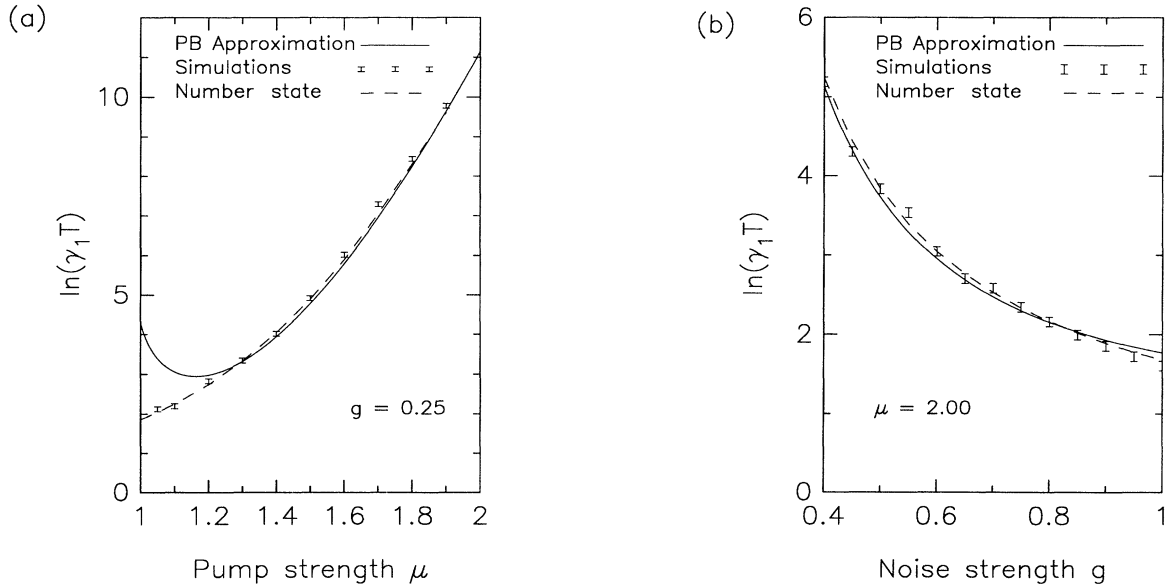

FIG. 4. Comparisons between the number-state and positive-P calculations. In (a), the pump strength μ is varied while the noise strength $g=0.25$, and in (b) the noise strength g is varied while the pump strength $\mu=2.00$. The potential-barrier (PB) approximation curve is the tunneling time predicted by Eq. (4.22), and the stochastic simulation points are obtained by numerical integration of Eqs. (4.3).

ison, the positive-P representation only gives second-order derivatives.

In the limit of large damping in the fundamental mode, an equation is obtained describing just the behavior of the subharmonic mode. This can be written in the scaled variables as

$$\frac{d}{d\tau}W(\beta,\tau)=\left[\frac{\partial}{\partial\beta}[\beta-\beta^*(\mu-g^2\beta^2)]+\frac{\partial}{\partial\beta^*}\{\beta^*-\beta[\mu-g^2(\beta^*)^2]\}+\frac{\partial^2}{\partial\beta\partial\beta^*}(1+2g^2\beta\beta^*)\right]W(\beta,\tau)\ . \quad (5.2)$$

The phase space of the Wigner distribution is a subspace of that of the positive-P distribution. The Wigner phase space is a single complex plane, and this is equivalent to the subspace of the positive-P phase space given by the relation $\alpha=\alpha^{\dagger *}$. Because of the presence of the bounded manifold in the positive-P phase space restricting the dynamics to real α and $\alpha^\dagger$, this means that the Wigner phase space is *orthogonal* to the positive-P bounded manifold. This does not imply any distinction in the physical behavior of the oscillator, since these representations simply provide a different computational technique. In either case, the relevant physical expectation values are obtained by averaging appropriate functions over the entire phase space. These will be identical in either representation, provided commutators are correctly taken into account when calculating the operator moments from the phase space moments.

We now separate β into its real and imaginary parts by writing $\beta=q+ip$, and so obtain the truncated Wigner Fokker-Planck equation and the corresponding set of Ito stochastic differential equations

$$\frac{d}{d\tau}W_T(q,p,\tau)=\left[\frac{\partial}{\partial q}\{q[1+g^2(q^2+p^2)-\mu]\}+\frac{\partial}{\partial p}\{p[1+g^2(q^2+p^2)+\mu]\}+\frac{1}{4}\left[\frac{\partial^2}{\partial q^2}+\frac{\partial^2}{\partial p^2}\right][1+2g^2(q^2+p^2)]\right]\times W_T(q,p,\tau)\ , \quad (5.3)$$

$$\begin{aligned} dq&=-q[1+g^2(q^2+p^2)-\mu]d\tau+\frac{1}{\sqrt{2}}[1+2g^2(q^2+p^2)]^{1/2}dZ_q\ ,\\ dp&=-p[1+g^2(q^2+p^2)+\mu]d\tau+\frac{1}{\sqrt{2}}[1+2g^2(q^2+p^2)]^{1/2}dZ_p\ . \end{aligned} \quad (5.4)$$

This truncated Wigner Fokker-Planck equation (5.3) does not have a potential solution, which makes analytic calculation of the tunneling time difficult. The effect of the quantum noise from the fundamental mode on the tunneling time can be included in a qualitative fashion if we restrict the problem to one dimesion, namely the q axis. One-dimensional Fokker-Planck equations always have a potential solution. This procedure is far from exact, but we note that the p component of the drift always points towards $p=0$, the q axis. The resulting Fokker-Planck equation in this approximation is

$$\frac{d}{d\tau}W_{1D}(q,\tau)=\left[\frac{\partial}{\partial q}[q(1+g^2q^2-\mu)]+\frac{1}{4}\frac{\partial^2}{\partial q^2}[1+2g^2q^2]\right]W_{1D}(q,\tau)\ . \quad (5.5)$$

This also generates a corresponding Ito stochastic differential equation, which is

$$dq=-q(1+g^2q^2-\mu)d\tau+\frac{1}{\sqrt{2}}(1+2g^2q^2)^{1/2}dZ_q\ . \quad (5.6)$$

The one-dimensional approximation gives the mean tunneling time in the potential barrier approximation as

$$T_{1D}=\frac{\pi}{\gamma_1}\left[\frac{2r+1}{2r^2}\right]^{1/2}\times\exp\left[\frac{1}{2g^2}[(2r+1)\ln|2r+1|-2r]\right]\ , \quad (5.7)$$

where

$$r=\mu-1-g^2\ .$$

Figures 5(a) and 5(b) show comparisons between these two types of stochastic equations, in addition to the number-state result and the one-dimensional truncated Wigner potential-barrier theory. In the range where the potential-barrier approximation is valid there is good agreement between the potential-barrier theory and the corresponding one-dimensional simulations. The full two-dimensional truncated Wigner simulations give consistently slightly shorter mean tunneling times than the one-dimensional simulations. This is expected since the two-dimensional simulations have an extra degree of freedom. The details of how the stochastic simulations were performed are given in Appendix B. As before, there is a divergence as the potential-barrier approximation fails near threshold, as the pump strength $\mu\rightarrow 1$ or as the noise strength $g\rightarrow 1$ [Figs. 5(a) and 5(b), respectively].

More interesting is the fact that both the truncated Wigner methods (one and two dimensional) give results that are inconsistent with the number-state method. Since the only extra approximation used by the two-dimensional simulations over the number-state results is the truncation of the third-order derivative terms, it is clear that these act to suppress the tunneling in this system. Thus, when they are removed, the tunneling time is artificially decreased. We emphasize that this must be an artifact of the truncation approximation. The eigenvalues of the full Wigner eequation necessarily agree with the other methods. Since the truncated Wigner equations are equivalent to stochastic electrodynamics, we conclude

that there is a fundamental *inequivalence* between this theory and the complete nonlinear quantum theory.

A two-dimensional potential solution to the truncated equations can also be obtained that is valid near threshold.[2] Here the noise contribution $2g^2(q^2+p^2)$ is small since both q and p are small. This term corresponds to vacuum fluctuations in the fundamental mode coupling through to the subharmonic mode. In this near-threshold approximation, this is neglected, leaving only the subharmonic noise. The Fokker-Planck equation and

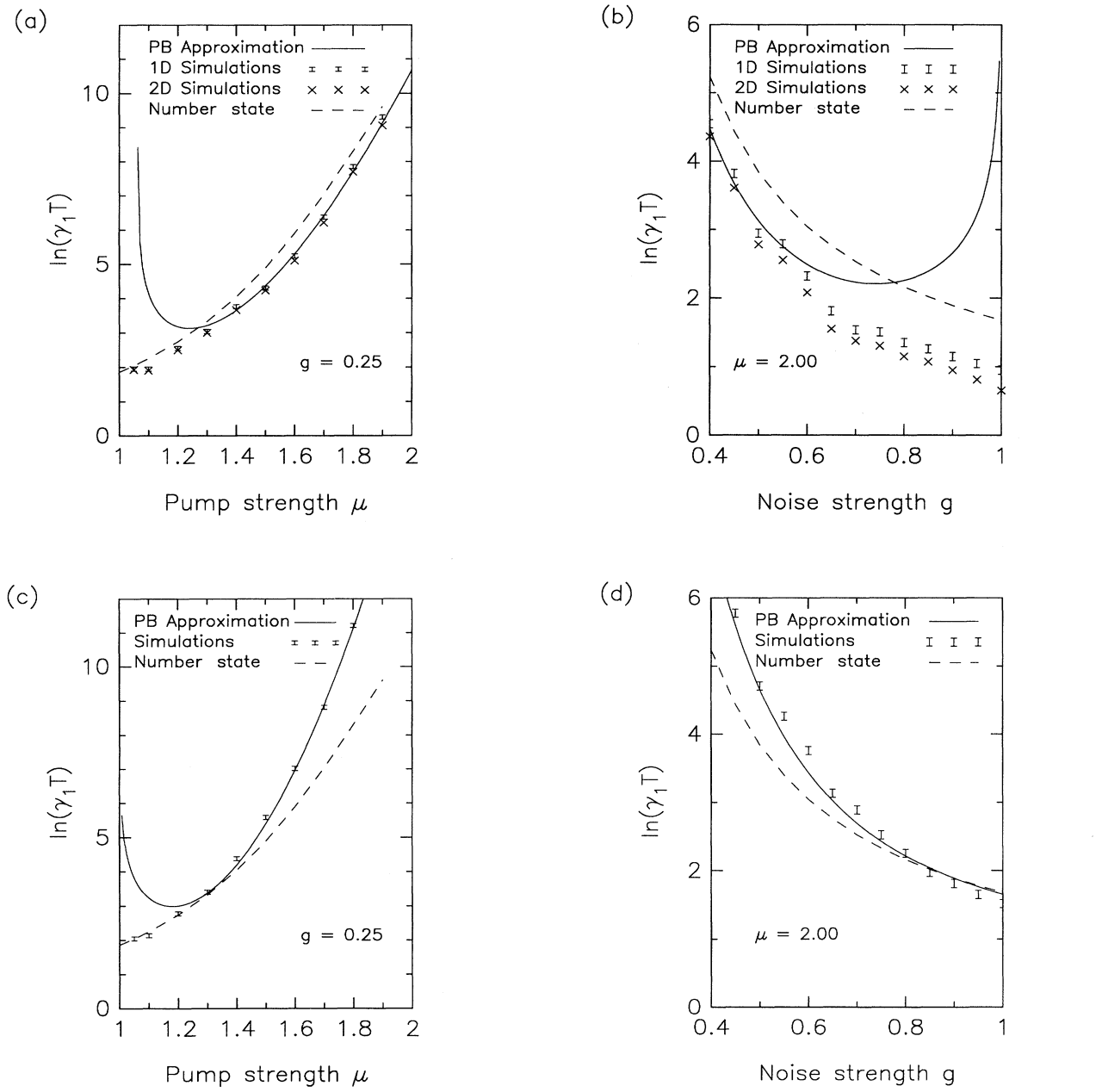

FIG. 5. Comparisons between the number-state and approximate Wigner calculations. Pump strength μ is varied in graphs (a) and (c) while the noise strength $g=0.25$. In graphs (b) and (d) the noise strength g is varied while the pump strength $\mu=2.00$. (a) and (b) show results obtained when the third-order derivative terms are truncated from the Wigner representation equation: the two-dimensional (2D) simulation and 1D simulation points are obtained by numerical integration of Eqs. (5.4) and (5.6), respectively. The potential-barrier (PB) approximation curve is given by Eq. (5.7). (c) and (d) show results when both third-order derivatives and noise from the fundamental mode are neglected, as in the near-threshold approximation. These simulation points are obtained by numerical integration of Eqs. (5.9), and the potential-barrier approximation curve is given by Eq. (5.11).

Ito equations are

$$\frac{d}{d\tau}W_{\rm NT}(q,p,\tau)=\left[\frac{\partial}{\partial q}\{q[1+g^2(q^2+p^2)-\mu]\}+\frac{\partial}{\partial p}\{p[1+g^2(q^2+p^2)+\mu]\}+\frac{1}{4}\left[\frac{\partial^2}{\partial q^2}+\frac{\partial^2}{\partial p^2}\right]\right]W_{\rm NT}(q,p,\tau)\ , \tag{5.8}$$

$$dq=-q[1+g^2(q^2+p^2)-\mu]d\tau+\frac{1}{\sqrt{2}}dZ_q\ ,$$
$$dp=-p[1+g^2(q^2+p^2)+\mu]d\tau+\frac{1}{\sqrt{2}}dZ_p\ . \tag{5.9}$$

With all the above approximations, the steady-state approximate Wigner distribution function $W_{\rm NT}(q,p)$ and potential $V_{\rm NT}(q,p)$ are

$$W_{\rm NT}(q,p)=N_{\rm NT}\exp[-V_{\rm NT}(q,p)]\ ,$$
$$V_{\rm NT}(q,p)=\frac{2}{g^2}[g^2q^2+g^2p^2+\tfrac{1}{2}(g^2q^2+g^2p^2)^2-\mu(g^2q^2-g^2p^2)]\ . \tag{5.10}$$

Here $N_{\rm NT}$ is normalization constant. Above threshold the potential has two minima, at $gq=\pm(\mu-1)^{1/2}$. In the limit of large threshold photon numbers (small noise strength g), these minima are very close to those obtained using the positive-P representation. After taking the different operator correspondences into account the near-threshold theory and the positive-P theory[7] predict identical results for small linear fluctuations near threshold. From the approximate Wigner distribution $W_{\rm NT}(q,p)$ we obtain the tunneling time by using the potential barrier approximation[26] to be

$$T_{\rm NT}=\frac{\pi}{\gamma_1}\left[\frac{\mu+1}{\mu(\mu-1)^2}\right]^{1/2}\exp\left[\frac{1}{g^2}(\mu-1)^2\right]\ . \tag{5.11}$$

Figures 5(c) and 5(d) illustrate the tunneling-time results obtained using the near-threshold approximation. As in the previous graphs, we see good agreement between the stochastic simulations and the corresponding potential-barrier theory. This agreement breaks down when near threshold as the pump strength $\mu\rightarrow 1$, or for large noise strength g, as the large potential-barrier approximation fails. From Fig. 5(c), it is clear that near threshold (pump strength $\mu=1$) the simulations agree with the number-state result, which is expected, since in this region the effects of the approximations are small. Far above threshold (pump strength $\mu\gg 1$), or for small noise g, these approximations give much *longer* tunneling times than the exact number-state results, because the neglected fundamental mode noise terms have a larger effect than the truncation approximation.

The exact quantum result in Eq. (4.22) scales as $\exp(2\mu/g^2)$ for pump strength $\mu\gg 1$, while the result of (5.11) scales as $\exp(\mu^2/g^2)$. This is similar to the difference between quantum tunneling through a barrier of height μ^2 and thermal activation over a barrier of the same height. In both cases, the difference becomes greater at large potential-barrier heights. This can be understood as being due to the extra approximations used to obtain (5.11), which effectively replace the quantum-mechanical problem by a classical thermal activation problem with an equivalent near-threshold behavior. The inclusion of the fundamental mode noise improves the theory somewhat, but even Eq. (5.3) is unable to reproduce the tunneling rate given by the quantum theory. However, if the third-order derivative terms are included by deriving the Wigner time evolution equation directly from the single-mode master equation (2.5), as has been recently done by Risken and Mortimer,[24] then agreement with the quantum results of Secs. III and IV can be regained.

VI. CONCLUSIONS

We have demonstrated good agreement between two exact methods of calculating the tunneling dynamics of the degenerate parametric oscillator. Both the number-state and coherent-state basis methods include the Hamiltonian nonlinearity exactly. Of course, either method is only applicable in regions where the original Hamiltonian is valid. Calculations using both analytical Fokker-Planck and numerical stochastic methods agree with the numerical solutions of the density-matrix master equation in the number-state basis. This serves to verify the accuracy and reliability of these different expansion techniques. The number-state and coherent-state methods are complementary from the computational point of view, with number-state expansions being more useful for low photon numbers, and coherent-state expansions being more useful in regions of large photon number.

In addition to this we have compared our results to those obtained using the Wigner representation, which should give exactly equivalent results. However, the use of the Wigner representation is accompanied by the introduction of extra approximations, to give more tractable equations. The first approximation is the truncation of third-order derivative terms from the time evolution equation. This results in a second-order Fokker-Planck equation, which is equivalent to stochastic electrodynamics. It gives *shorter* mean tunneling times than the exact methods, evidently due to the effect of the truncation approximation. When noise from the fundamental mode is also neglected, as in the near-threshold approximation, a classical potential problem is obtained giving *longer* mean tunneling times than the exact methods. This difference can be compared with the quantum penetration of a potential barrier, which is much faster than classical thermal activation at large barrier heights.

A summary of the results from Secs. III–V is shown in Fig. 6, where all the stochastic simulations are compared with the number-state calculations. These graphs show the *difference* between the results from the simulations and the number-state results. The positive-P stochastic simulations agree with the number-state calculations. The truncated Wigner (stochastic electrodynamics) simulations always give *shorter* mean tunneling times than the

number-state or positive-P results. The simulations using the near-threshold approximations usually give longer tunneling times than the number-state calculations, because the extra noise from the fundamental mode is neglected. Very near threshold (pump strength $\mu \approx 1$), all the methods tend to agree, as is shown in Appendix C. This is expected from known general results on the representation invariance of tunneling near critical and turning points.[31]

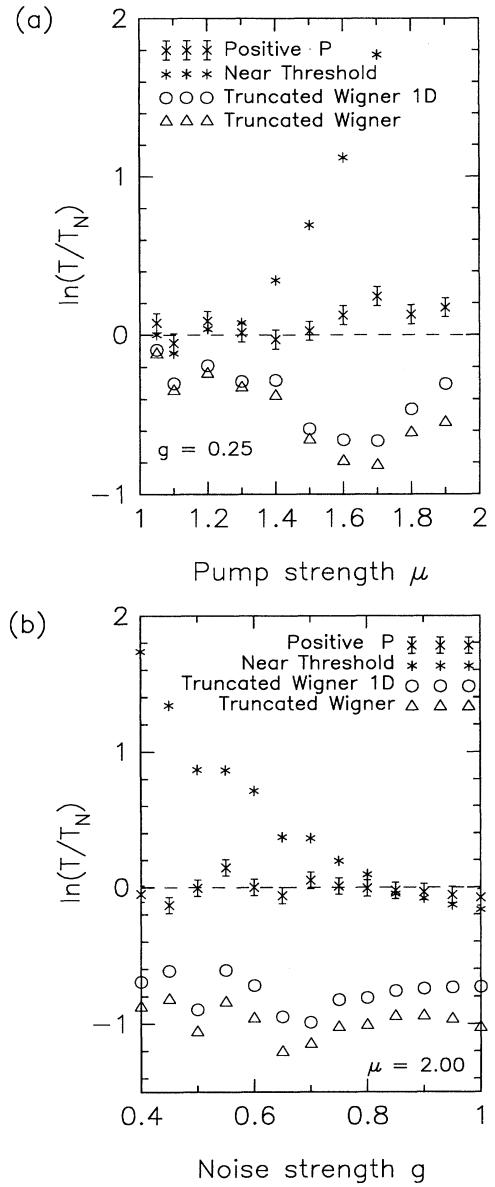

FIG. 6. Comparisons between the number-state results and all types of stochastic simulation. The points are plotted as $\ln(T/T_N)$, where T_N is the number-state tunneling time. In (a), the pump strength μ is varied while the noise strength $g=0.25$ and in (b) the noise strength g is varied while the pump strength $\mu=2.00$. Error bars are only shown on the positive-P results for clarity, but the errors for all the stochastic results are of similar magnitude. The positive-P stochastic simulation points are obtained by numerical integration of Eqs. (4.3). The truncated Wigner and 1D truncated Wigner simulation points are obtained by numerical integration of Eqs. (5.4) and (5.6), respectively. The near-threshold approximation simulation points are obtained by numerical integration of Eqs. (5.9).

We note an intriguing subtlety in the interplay of these different results. The quantum equations of the coherent-state positive-P representation have an exact potential solution. Solutions for nonequilibrium quantum problems are rare: this model is therefore a useful test for investigating nonequilibrium quantum effects. On the other hand, the truncated Wigner equations have no exact potential solution. Thus the effect of restricting this quantum problem to a classical phase space destroys an essential symmetry in the equations. The nonclassical phase space of the positive-P distribution allows the equations to have an exact potential solution. This potential solution is not the same as that previously obtained using semiclassical methods by eliminating the noise in the fundamental mode, even though it does predict similar behavior near threshold.

Above threshold, the potential solution in the positive-P representation predicts much faster tunneling than that obtained previously. This is a quantum effect, which is obtained here through off-diagonal coherent-state expansions of the density matrix. It might be thought that the correct result could be regained by inclusion of the fundamental mode noise in the Wigner representation equations—but this is not the case. The neglect of third-order derivative terms occurring in the Wigner representation means that even this does not give correct tunneling rates. The third-order terms are associated with negative valued Wigner functions and quantum interference. Thus the fact that they suppress tunneling suggests that these represent destructive quantum interference of the noise terms, with no classical counterpart.

Despite the well-known nature and experimental significance of the quantum parametric amplifier,[32] *all* these results are unprecedented, except for those in Graham's original work. In the case treated here, there is only one mode involved, although it is coupled to reservoirs. More complicated multimode cases are even less well known. Thus nonequilibrium quantum systems remain the least-well-understood quantum systems. The exact quantum theory gives shorter mean tunneling times than previously obtained—and longer mean tunneling times than a full stochastic electrodynamics theory. With recent developments in Josephson-junction parametric amplifiers[33] this should become testable in the near future.

APPENDIX A: NUMERICAL NUMBER-STATE TECHNIQUES

The tunneling eigenvalues are found by calculating the eigenvalues of the transition matrix in double precision using FORTRAN software.[34] These numerical routines first balance the transition matrix, reduce it to upper Hessenberg form, and then find its eigenvalues and eigenvectors.[35] As an independent check on the software, we compared some of the results with those obtained using

different hardware and an alternative software library.[36] All the sets of results could not be compared in this way because of time and memory constraints. The comparisons that were made produced good agreement.

To check the numerical accuracy of the answers, we also tested for convergence. That is, we calculated the eigenvalues for a particular maximum photon number N, and then recalculated the data using $N+1$. If there was no significant change in the eigenvalue, then clearly the truncation of the transition matrix had little effect. These changes were typically kept to much less than 1%. An extra accuracy check was performed by multiplying the steady-state and tunneling eigenvectors with the transition matrix and comparing it with the expected result, which is the eigenvalue times the eigenvector. The difference is a measure of the error. In all cases we ensured that this error remained less than one part in 10^4, and in most cases it was orders of magnitude smaller. Although only 15-decimal, double precision arithmetic was used, the reproducibility of the results using different software persuades us that round-off error was negligible.

APPENDIX B: STOCHASTIC CALCULATIONS

In order to solve the Ito stochastic differential equations, which are differential equations with randomly varying coefficients, an iterated central difference method was used.[37,38] The tunneling eigenvalue is equivalent to the slowest decay rate of the amplitude α in the subharmonic mode. To obtain the required data, a FORTRAN program that calculated the evolution of a large ensemble of trajectories in parallel was written. The Gaussian noises were generated by means of an appropriately weighted and scaled pseudorandom number generator.[39] At intervals during execution of the program, the ensemble averaged amplitude $\langle\alpha\rangle$, together with the elapsed time, were saved. All of the trajectories were started at the classical stable state specified by the pump strength μ, with no initial spread. This corresponds to an initial coherent state with $g^2\alpha^2=\mu-1+g^2$ in the case of the positive-P representation. However, the exact details of the initial distribution have little effect on the decay of the ensemble averaged amplitude, since the relaxation of the initial δ function to the single-well distribution occurs on a much shorter time scale than tunneling between wells. The exponential decay of $\langle\alpha\rangle$ meant that the tunneling eigenvalue could be extracted from the data by using logarithmic regression.

To check the convergence of these stochastic simulations we used the standard technique of varying the time resolution. If the change in the calculated eigenvalue was less than 1% when the time step was doubled, then the simulation result was considered to be accurate. Typical time steps used were $\gamma_1/128$ and $\gamma_1/256$. In order to test convergence it is essential that each trajectory and its lower-resolution counterpart are driven by Gaussian noise sampled from identical underlying noise trajectories, as is described elsewhere.[38] The errors in the results were estimated by treating each tunneling event (of a trajectory) as a Poisson process. Given this assumption, the relative error in the eigenvalue is proportional to $n^{-1/2}$, where n is the number of tunneling events. Typically we calculated many trajectories in parallel, allowing sufficient time for at least 256 of the 1024 trajectories in the ensemble to tunnel. The error estimate for the stochastic simulation results is thus about 6%, as is indicated in Figs. 4–6. We tested this by calculating the standard deviation of an ensemble of eigenvalues that had been obtained for a particular set of parameters. The standard deviation of the ensemble of eigenvalues was in agreement with our error estimate.

APPENDIX C: NEAR-THRESHOLD COMPARISONS

In this appendix we compare the near-threshold potential barrier heights in the limit of large photon number for each of the three potential solutions. The potential-barrier height for the positive-P representation using the constant diffusion variables u and v is given by

$$\Delta U=\frac{2}{g^2}[\mu-\bar{\sigma}-\bar{\sigma}\ln(\mu/\bar{\sigma})]\ . \tag{C1}$$

We take the near-threshold limit by putting the pump strength $\mu=1+\zeta$, and taking $|\zeta|\ll 1$. The classical, large-photon-number limit is taken by letting the noise strength $g\to 0$. Using these, the potential barrier height is

$$\Delta U=\frac{2}{g^2}[\zeta-\ln(1+\zeta)]\ . \tag{C2}$$

When the logarithmic term is expanded for small ζ, we get

$$\Delta U=\frac{1}{g^2}\zeta^2-\frac{2}{3g^2}\zeta^3+\cdots\ . \tag{C3}$$

The one-dimensional truncated Wigner potential gives a barrier height of

$$\Delta V_{1D}=\frac{1}{2g^2}[(2r+1)\ln(2r+1)-2r]\ , \tag{C4}$$

where r has been defined in Eq. (5.7). Using the same limits as above, this reduces to

$$\Delta V_{1D}=\frac{1}{g^2}\zeta^2-\frac{2}{3g^2}\zeta^3+\cdots\ . \tag{C5}$$

However, note that the ζ^4 term in (C5) is different from that for the positive-P representation. For the near-threshold potential, we have the potential barrier height equal to

$$\Delta V_{NT}=\frac{1}{g^2}(\mu-1)^2\ , \tag{C6}$$

which reduces in the near-threshold and classical limits to

$$\Delta V_{\mathrm{NT}} = \frac{\zeta^2}{g^2} \ . \tag{C7}$$

So, to leading order, all these calculations for the different potentials give equivalent near-threshold behavior in the large-photon-number limit. The near-threshold potential barrier expansion has no term in ζ^3 due to the omission of the fundamental mode noise. This directly results in the slower tunneling above threshold, as is explained in the text.

[1]J. W. F. Woo and R. Landauer, IEEE J. Quantum Electron. **7**, 435 (1971).

[2]R. Graham, in *Quantum Statistics in Optics and Solid-State Physics,* edited by G. Hohler, Springer Tracts in Modern Physics, Vol. 66 (Springer, New York, 1973), p. 1.

[3]A. O. Caldeira and A. J. Leggett, Ann. Phys. (N.Y.) **149**, 374 (1983).

[4]R. J. Cook and H. J. Kimble, Phys. Rev. Lett. **54**, 1023 (1985).

[5]E. P. Wigner, Phys. Rev. **40**, 749 (1932).

[6]P. Kinsler and P. D. Drummond, Phys. Rev. Lett. **64**, 236 (1990).

[7]P. D. Drummond, and P. Kinsler, Phys. Rev. A **40**, 4813 (1989).

[8]P. D. Drummond and C. W. Gardiner, J. Phys. A **13**, 2353 (1980).

[9]T. W. Marhsall, Proc. R. Soc. London, Ser. A **276**, 475 (1963). See also the review by T. H. Boyer, in *Foundations of Radiation Theory and Quantum Electrodynamics,* edited by A. O. Barut (Plenum, New York, 1980).

[10]P. D. Drummond, K. J. McNeil, and D. F. Walls, Opt. Acta **28**, 211 (1981).

[11]W. H. Louisell, *Quantum Statistical Properties of Radiation* (Wiley, New York, 1973).

[12]H. Carmichael and M. Wolinsky, in *Quantum Optics IV,* edited by J. D. Harvey, and D. F. Walls (Springer, Berlin, 1986), p. 208.

[13]E. Schrödinger, Naturwissenschaften **14**, 644 (1927).

[14]R. J. Glauber, Phys. Rev. **130**, 2529 (1963).

[15]E. C. G. Sudarshan, Phys. Rev. Lett. **10**, 277 (1963).

[16]K. J. McNeil and C. W. Gardiner, Phys. Rev. A **28**, 1560 (1983).

[17]M. D. Reid and P. D. Drummond, Phys. Rev. Lett. **60**, 2731 (1988).

[18]M. D. Reid and P. D. Drummond, Phys. Rev. A **40**, 4493 (1989).

[19]P. D. Drummond and M. D. Reid, Phys. Rev. A **41**, 3930 (1990).

[20]M. D. Reid and D. F. Walls, Phys. Rev. A **33**, 4465 (1986).

[21]R. E. Slusher, L. W. Hollberg, B. Yurke, J. C. Mertz, and J. F. Valley, Phys. Rev. Lett. **55**, 2409 (1985).

[22]A. M. Smith and C. W. Gardiner, Phys. Rev. A **39**, 3511 (1989).

[23]L. Arnold, *Stochastic Differential Equations: Theory and Applications* (Wiley, New York, 1974); C. W. Gardiner, *Handbook of Stochastic Methods* (Springer, Berlin, 1983).

[24]I. K. Mortimer and H. Risken, Phys. Rev. A (to be published).

[25]M. Wolinsky and H. J. Carmichael, Phys. Rev. Lett. **60**, 1836 (1988).

[26]H. A. Kramers, Physica **7**, 284 (1940); R. Landauer and J. A. Swanson, Phys. Rev. **121**, 1668 (1961).

[27]H. Haken, Rev. Mod. Phys. **47**, 67 (1975).

[28]M. Hillery, R. F. O'Connell, M. O. Scully, and E. P. Wigner, Phys. Rep. **106**, 121 (1984).

[29]S. Reynaud, C. Fabre, and E. Giacobino, J. Opt. Soc. Am. B **4**, 1520 (1987).

[30]Ning Lu, Shi-Yao Zhu, and G. S. Agarwal, Phys. Rev. A **40**, 258 (1989).

[31]P. D. Drummond, Phys. Rev. A **33**, 4462 (1986).

[32]L. Wu, H. J. Kimble, J. L. Hall, and H. Wu, Phys. Rev. Lett. **57**, 2520 (1986).

[33]B. Yurke, L. R. Corruccini, P. G. Kaminsky, L. W. Rupp, A. D. Smith, A. H. Silver, R. W. Simon, and E. A. Whittaker, Phys. Rev. A **39**, 2519 (1989).

[34]The calculations were carried out on an Apollo DN10000, using 64-bit real arithmetic with a 52-bit mantissa (IEEE standard). The software subroutines for calculating eigenvalues and eigenvectors were obtained from the public domain network source "Netlib." We used the EISPACK routines, originally developed by the NATS project at Argonne National Laboratory. These in turn are identical to those algorithms described in Ref. 35.

[35]J. H. Wilkinson and C. Reinsch, *Handbook for Automatic Computation* (Springer, Berlin, 1971), Vol. 2.

[36]These calculations were carried out on a Digital Equipment Corporation Vax 11/750, using DEC 64-bit real arithmetic with a 55-bit mantissa. The software subroutines for calculating eigenvalues and eigenvectors were obtained from the Numerical Algorithms Group, Wilkinson House, Jordan Hill Road, Oxford OX2 8DR, United Kingdom. These are identical to those algorithms described in Ref. 35.

[37]P. D. Drummond, Comput. Phys. Commun. **29**, 211 (1983).

[38]P. D. Drummond and I. K. Mortimer, J. Comput. Phys. **93**, 144 (1991).

[39]A pair of real Gaussian random numbers s_1, s_2 can be obtained from a pair of real random numbers r_1, r_2 in the range $(-1, +1)$ by using the Box-Mueller formula $s_i = r_i z$ where

$$z = \{[-2\ln(1-r_1^2-r_2^2)]/(r_1^2+r_2^2)\}^{1/2} \ .$$